ACS APPLIED MATERIALS & INTERFACES

www.acsami.org

Research Article

Out-of-Plane Deformations Determined Mechanics of Vanadium Disulfide (VS_2) Sheets

Guorui Wang, Zhepeng Zhang, Yanlei Wang, Enlai Gao, Xiangzheng Jia, Zhaohe Dai, Chuanxin Weng, Luqi Liu,* Yanfeng Zhang, and Zhong Zhang*

Cite This: *ACS Appl. Mater. Interfaces* 2021, 13, 3040−3050

Read Online

ACCESS | Metrics & More | Article Recommendations | Supporting Information

ABSTRACT: The rapid development of two-dimensional (2D) materials has significantly broadened the scope of 2D science in both fundamental scientific interests and emerging technological applications, wherein the mechanical properties play an indispensably key role. Nevertheless, particularly challenging is the ultrathin nature of 2D materials that makes their manipulations and characterizations considerably difficult. Herein, thanks to the excellent flexibility of vanadium disulfide (VS_2) sheets, their susceptibility to out-of-plane deformation is exploited to realize the controllable loading and enable the accurate measurements of mechanical properties. In particular, the Young's modulus is estimated to be 44.4 ± 3.5 GPa, approaching the lower limit for 2D transition metal dichalcogenides (TMDs). We further report the first measurement of thickness-dependent bending rigidity of VS_2, which deviates from the prediction of the classical continuum mechanics theory. Additionally, a deeper understanding of the mechanics within two dimensions also facilitates the modulation of strain-coupled physics at the nanoscale. Our Raman measurements showed the Grüneisen parameters for VS_2 were determined for the first time to be $\gamma_{E_{2g}^1} \approx 0.83$ and $\gamma_{A1g} \approx 0.32$.

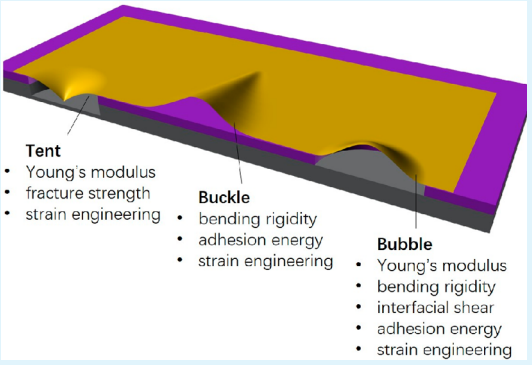

KEYWORDS: *two-dimensional (2D) materials, vanadium disulfide nanosheet, out-of-plane deformation, nanomechanics, strain engineering*

INTRODUCTION

The rapid progress in graphene research has fueled vigorous scientific inquiry in novel two-dimensional (2D) materials. Known for the atomic thickness combined with the van der Waals (vdW) interaction among the layers, 2D materials with extreme bendability energetically favor out-of-plane elastic deformations when subject to mechanical stimuli, giving rise to rich morphologies such as wrinkles,[1,2] buckles,[3,4] bubbles,[5,6] tents,[7,8] folds,[9,10] and scrolls.[11,12] These out-of-plane deformation modes, in turn, grant the feasible access to understand the mechanical properties and interfacial interactions of 2D materials. These understandings may further enable the structural design and interface engineering for applications ranging from functional composites to flexible electronics.[13−15] In addition, the considerable local strain associated with out-of-plane deformation gives rise to tunable physical characteristics of 2D materials, termed strain engineering.[16,17] In these regards, out-of-plane deformation modes, though not always favored in 2D material devices, can offer experimental platforms to explore the mechanics of 2D materials as well as its interplay with electronics or optics.

Three typical out-of-plane deformation modes, including poking, bubbling, and buckling shown in Figure 1, are frequently involved to determine the key mechanical parameters of 2D materials. For instance, poking suspended membranes with (inverse) tentlike deformations via atomic force microscopy (AFM) nanoindentation represents a reliable yet facile way to measure Young's modulus and fracture strength of 2D materials.[18−21] The bulge test generates a uniform global strain field, allowing the determination of elastic properties such as Young's modulus and bending rigidity.[22−24] Our early work has proven that the extracted average Young's moduli of multilayer graphene, hBN, and MoS_2 agree well with those measured by AFM nanoindentation.[23] Additionally, because of considerably weak vdW bonding at the interface, delamination always occurs prior to the failure of 2D materials upon increasing pressure, thus enabling the bulge test to estimate the interfacial adhesion energy instead of fracture strength. Buckling instability is an extensively observed deformation mode in 2D materials due to

Received: November 5, 2020
Accepted: December 21, 2020
Published: January 5, 2021

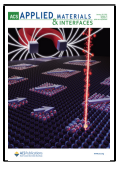

https://dx.doi.org/10.1021/acsami.0c19835
ACS Appl. Mater. Interfaces 2021, 13, 3040−3050

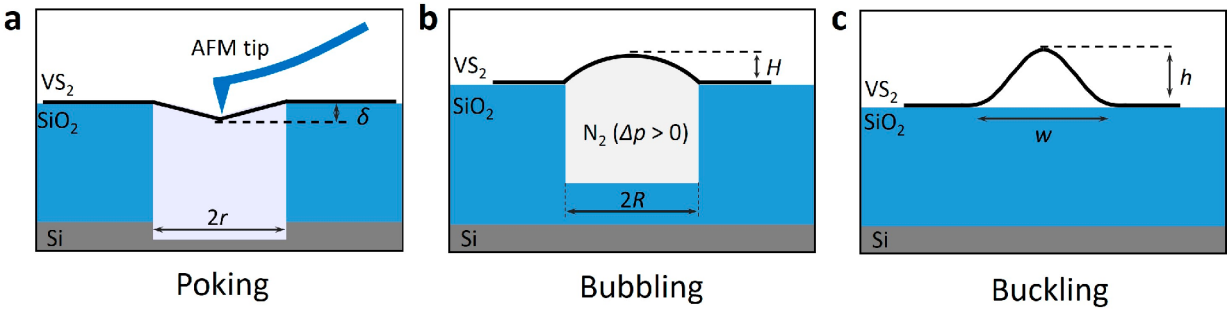

Figure 1. Schematics of typical out-of-plane deformation modes for mechanical characterizations, including (a) poking, (b) bubbling, and (c) buckling.

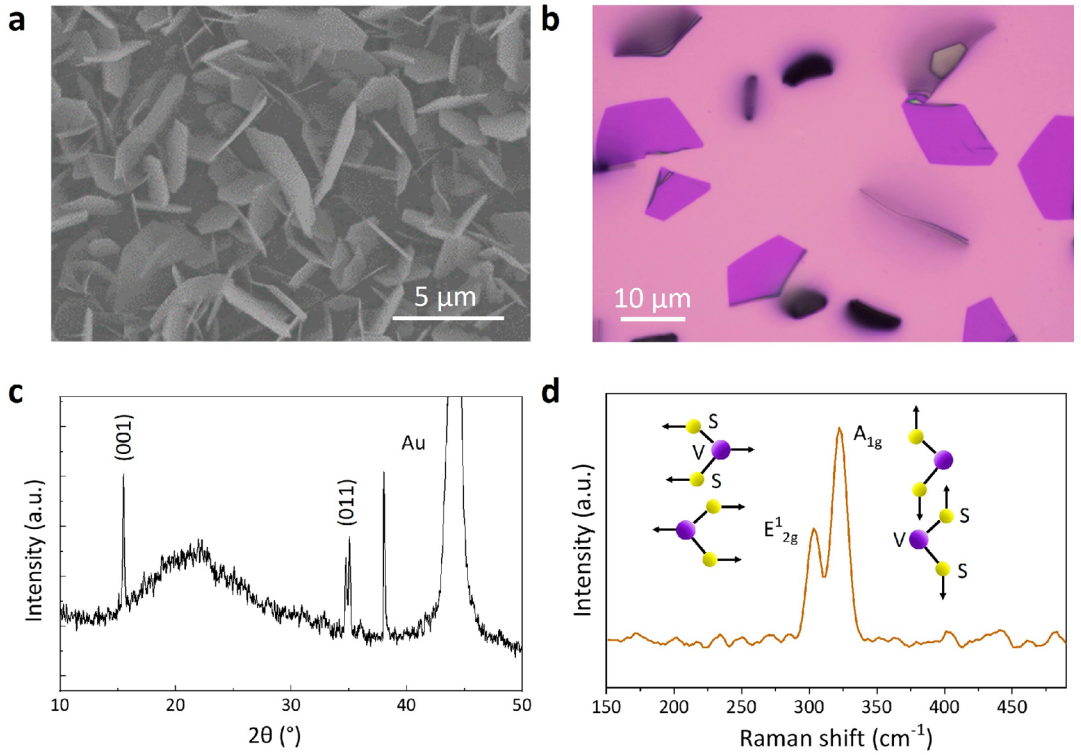

Figure 2. (a) Scanning electron microscope (SEM) image of VS_2 nanosheets vertically grown on SiO_2/Si substrate. (b) Optical micrograph, (c) XRD patterns, and (d) Raman spectra of VS_2 nanosheets.

their thinness.[25] The formation of buckles indicates the release of global in-plane strains that typically come from mechanical deformations (e.g., compression, prestretch/release), thermal stress (e.g., CVD growth), or lattice mismatch (e.g., epitaxy and transfer).[17] The underlying mechanism rests with the competition between the elastic strain energy of the 2D material and interfacial energy, which makes it possible to determine the elastic or interfacial parameters based on the geometrical parameters of the buckle profile.

Analogous to graphene, 2D transition metal dichalcogenides (TMDs) have exhibited glaringly distinctive physical properties compared with conventional semiconductor materials and their bulk counterparts. Within the family of TMDs, vanadium disulfide (VS_2) with triangularly packed layers of vanadium atoms sandwiched between two layers of S atoms is a typical metallic member without a bandgap in its electronic structure.[26,27] Recent theoretical works have unraveled that VS_2 possesses intrinsic magnetic ordering, which renders it the first 2D ferromagnet that stands out from other TMDs and holds promise for next-generation spintronic devices.[28,29] Furthermore, it is anticipated that the bandgaps, ferromagnetic properties, and even phase structures of VS_2 can be effectively regulated by mechanical strains,[30,31] thus inviting new opportunities in electronics, spintronics, and so forth. Unfortunately, though complementing the extensive efforts in the synthesis as well as physical and chemical properties of VS_2,[32,33] the mechanical studies such as the measurement of elastic properties have remained unexplored yet.

In this work, we successfully extracted the key mechanical parameters of VS_2 based on three out-of-plane deformation modes as mentioned in Figure 1. Specifically, elastic modulus and fracture strength of VS_2 nanosheets were derived from the AFM nanoindentation test. The interfacial energy between VS_2 and SiO_2/Si substrate was obtained from the bubbling-induced delamination test. More importantly, for multilayer 2D materials, the bending deformation dominates the elastic energy;[34] thus, the buckling paves a pathway for estimating the thickness-dependent bending rigidity of 2D materials. While

https://dx.doi.org/10.1021/acsami.0c19835
ACS Appl. Mater. Interfaces 2021, 13, 3040−3050

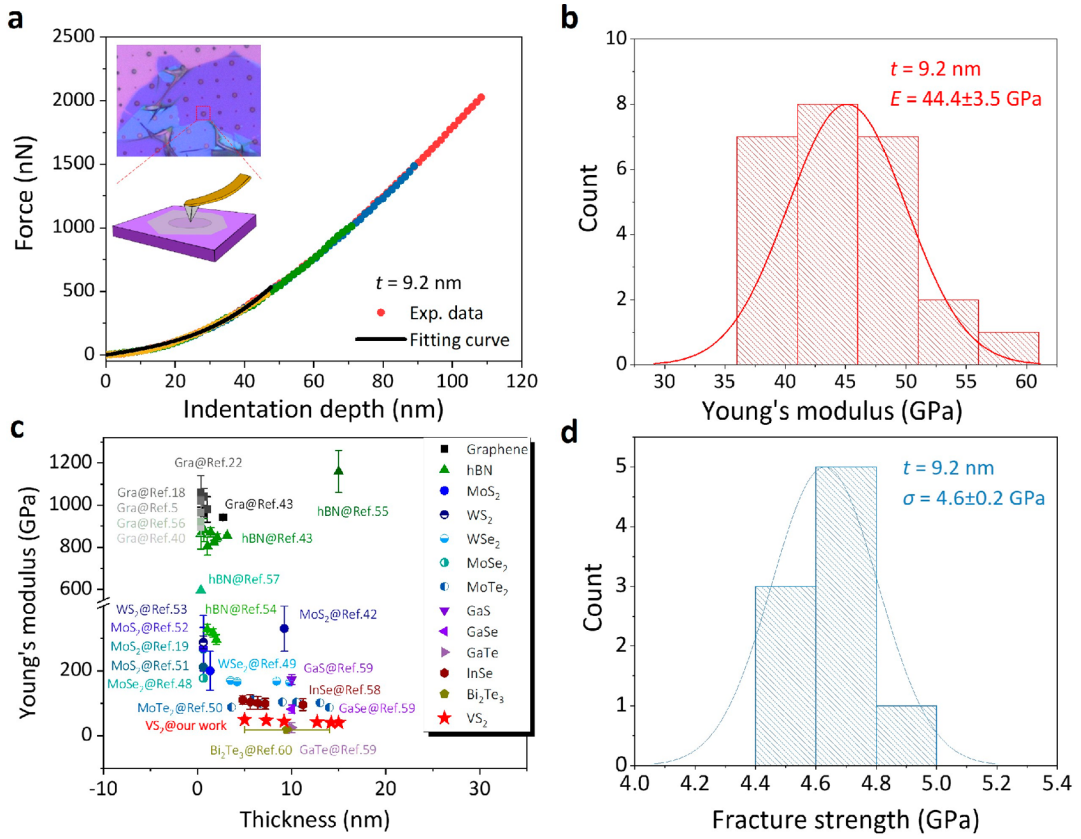

Figure 3. (a) Consecutive force vs deflection curve acquired at the center of freely suspended VS_2 nanosheet with a thickness of 9.2 nm under different loads. The inset is an optical micrograph of VS_2 nanosheets deposited on SiO_2/Si substrate patterned with arrays of cavities. Schematic diagram shows the indentation test performed with the tip of an atomic force microscope. (b) Histogram of Young's modulus for VS_2 nanosheet with a thickness of 9.2 nm. (c) Comparison of Young's moduli for VS_2 nanosheets and other 2D materials with different thicknesses. (d) Histogram of fracture strength of VS_2 nanosheet with a thickness of 9.2 nm.

the bulge test requires platelike deformation characteristics to allow for the measurement of bending rigidity, which is challenging to achieve for compliant materials (e.g., VS_2), the buckle-based approach works more efficiently with a broader scope of materials. We note that by using soft polymeric substrates, wrinkling may form to provide an alternative way to estimate the film's stiffness.[35] However, this method is precluded when the substrate is rigid, such as SiO_2/Si in this work. We thus focus only on the buckle delamination of the VS_2 sheets here. Besides the derived intrinsic mechanical parameters of VS_2 nanosheet, we further present an example for bulge test directed strain engineering reflected by Raman responses to evaluate the Grüneisen parameter, which is one of key parameters in determining thermodynamic properties of 2D materials ranging from the phonon frequency shift to thermal expansion. In contrast to buckles typically with unpredicted strains, the bulge test offers a higher controllability over the strain level and distribution, allowing continuous modulation of physics in 2D materials. Our results not only shed light on the mechanical response of 2D VS_2 sheets to out-of-plane deformations but also offer direct guidelines for the optimal design for their strain engineering applications. These out-of-plane metrologies, however, are not limited to VS_2 sheets and may be applicable to other thin crystalline film more broadly.

RESULTS AND DISCUSSION

Characterization of 2D VS_2 Nanosheets. The VS_2 samples studied in the current work are identical with those reported in previous work,[26] where VS_2 was vertically grown on the SiO_2/Si substrate by an ambient-pressure CVD method as shown in Figure 2a. Their sizes and thicknesses can be finely controlled by tuning concentrations of gaseous feedstocks. Both the X-ray photoelectron spectroscopy (XPS) and transmission electron microscopy (TEM) characterization determined the chemical composition of the VS_2 nanosheets.[26] To benefit the structural characterization and further operation, such vertically grown 2D VS_2 nanosheets were mechanically pressed facedown onto the SiO_2/Si substrate. The purple contrasts of the optical image in Figure 2b also demonstrate their ultrathin nature. X-ray diffraction (XRD) was used to resolve the crystal structure of the VS_2 nanosheets deposited on the gold substrate. We can clearly identify two main diffraction peaks corresponding to (001) and (011) from VS_2 crystals as shown in Figure 2c, which agrees with the one reported in the literature of VS_2 nanosheets synthesized by using the CVD method.[27,36] Specifically, the (001) peak at $2\theta = 15.52°$ corresponds to a d-spacing of ~5.703 Å. This is within 1.0% of the theoretical $d(001)$-spacing of 5.755 Å,[37,38] indicating that the possible presence of interstitial V atoms within the van der Waals gap introduced negligible distortion in the 1T-phase atomic structure of VS_2.[26] Figure 2d presents the Raman spectrum of VS_2 nanosheets prepared on SiO_2/Si substrate. Two characteristic peaks can be observed, including

https://dx.doi.org/10.1021/acsami.0c19835
ACS Appl. Mater. Interfaces 2021, 13, 3040−3050

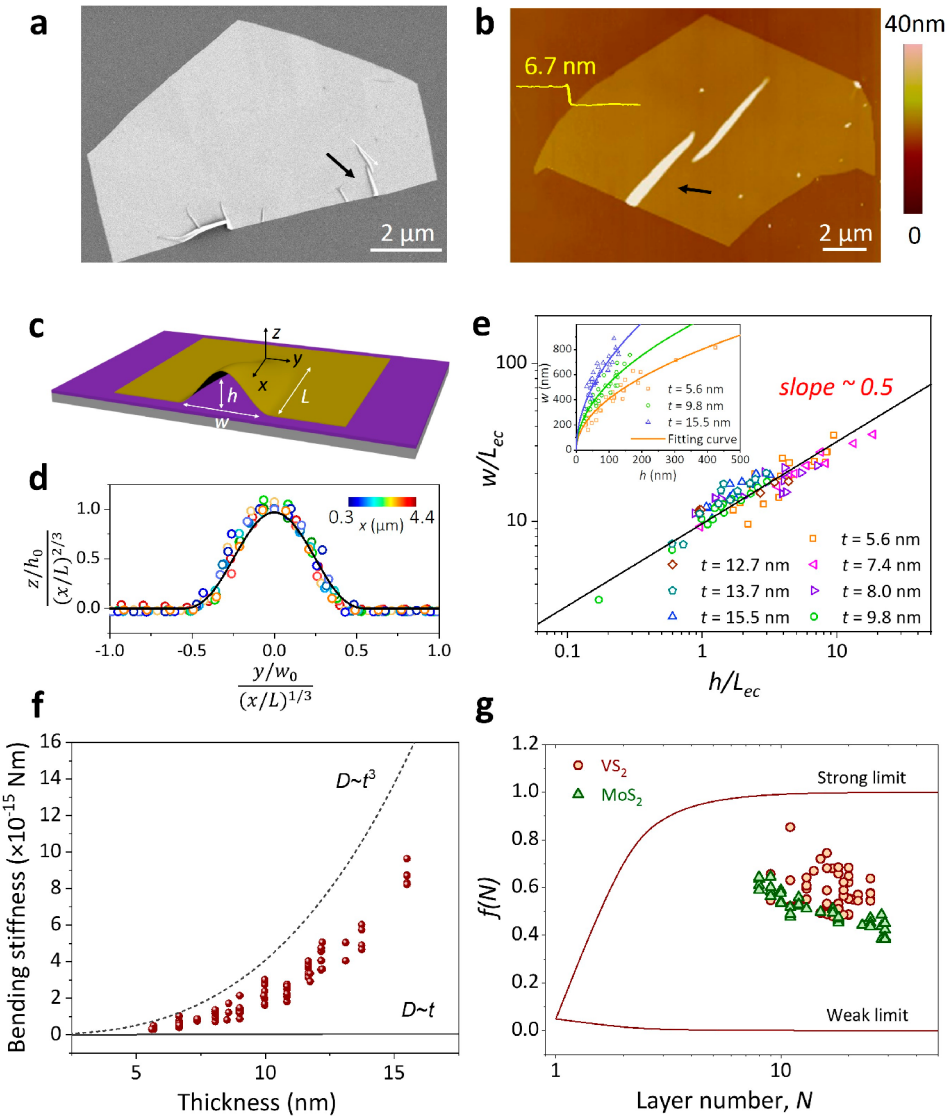

Figure 4. (a) SEM image and (b) AFM image of VS_2 nanosheets with different shapes transferred onto a SiO_2/Si substrate, featuring tiny buckles at varying widths especially on the edges. (c) Schematic illustration of the buckled VS_2 nanosheet on a SiO_2/Si substrate. The buckle lies along a straight direction, with a slowly varying width and a finite length L. The terms h and w stand for the amplitude and wavelength of the buckle, respectively. (d) Profiles of the successive sections of the same buckle represented in the normalized coordinates. h_0 and w_0 are the amplitude and wavelength of the buckle at the edge of nanosheet. (e) Normalized width as a function of normalized amplitude for VS_2 nanosheets with different thicknesses and initial transverse displacements. The solid line corresponds to a power law fit with an exponent of 1/2 (eq 3). The inset is the dimensional data, where colored symbols are used to differentiate the samples with the same thickness. (f) Thickness-dependent bending rigidity of VS_2 nanosheets. Dashed and solid lines are theoretical predictions for the perfectly bonding ($D \sim t^3$) and perfectly lubricated ($D \sim t$) cases, respectively. (g) Layer-dependent function $f(N)$ to measure the effect of interlayer coupling on the bending rigidity of multilayers.

the in-plane (E^1_{2g}) mode at 299.9 cm^{-1} and the out-of-plane (A_{1g}) mode at 322.3 cm^{-1}, which are aligned with reported values for VS_2.[27,39] The structural information provided by Raman spectra demonstrates as well that V intercalation did not induce apparent lattice distortion in VS_2 frameworks. Through AFM measurements, the thickness of VS_2 nanosheets studied in our work was accurately determined, ranging from 5.0 to 18.2 nm accompanying the layer number from ~8 to ~28.

Measurement of Young's Modulus and Fracture Strength of VS_2. VS_2 nanosheets with various thicknesses were transferred to SiO_2/Si substrate patterned with arrays of cavities (Figure 3a, inset). We use the tapping mode to locate the sample position before the nanoindentation test. Then, commercially available tips with a hemispherical geometry (radius: 40 nm) and low wear coating were employed to indent the suspended VS_2 nanosheet at the center.[40] Figure 3a displays typical force−displacement curves within four loading cycles performed on the same VS_2 nanosheet (thickness of 9.2 nm), with an incremental loading of 500 nN. The resulting curves show high recoverability, implying that inelastic deformation such as the plasticity and the interfacial slippage can be negligible.

Generally, the indentation process was modeled as a clamped circular membrane subject to a central point load. The loading curve can be divided into two stages as manifested by a logarithmic scale in Figure S1a.[41,42] At relatively low indentation depth (0.1−10 nm), the force−displacement curve appears to be linear, wherein the associated stiffness is governed by the pretension and the bending rigidity of VS_2

https://dx.doi.org/10.1021/acsami.0c19835
ACS Appl. Mater. Interfaces 2021, 13, 3040−3050

nanosheet. At large indentation depth, the in-plane stretching becomes dominated, and the force is proportional to the cubic displacement. An approximation was given[42]

$$F = \left[\frac{4\pi E}{3(1-\nu^2)}\frac{t^3}{r^2}\right]\delta + (\pi\sigma_0^{2D})\delta + \left(\frac{q^3 Et}{r^2}\right)\delta^3 \quad (1)$$

where F is the applied load, E is Young's modulus, ν is Poisson's ratio, t is the thickness of nanosheet, r is the hole radius, σ_0^{2D} is the pretension, and $q = 1/(1.05 - 0.15\nu - 0.16\nu^2)$ is a constant relating to ν of the sheet parameter. Our first-principles calculation result gives the averaged Poisson's ratio $\nu = 0.32$ so that $q \approx 1$ (see details in Figure S3). It is noteworthy that even for thick VS_2 nanosheets (Figure S1), we still can observe the membrane characteristics ($F \sim \delta^3$) at an efficient indenting depth. Of particular interest is hence to extract the coefficient of the cubic term in eq 1 that gives rise to the estimation of Young's modulus. As highlighted by the black curve in Figure 3a, eq 1 offers a good fit for the experimental data with high precision ($R^2 > 0.995$). The histogram of extracted Young's moduli is presented in Figure 3b, with an average of 44.4 ± 3.5 GPa based on the measurements of 25 different samples with $t = 9.2$ nm. Interestingly, the obtained Young's modulus is almost independent of the sample thickness, which slightly decreases from 49.6 ± 7.4 GPa to 40.3 ± 8.4 GPa as thickness increases from 5.0 nm to 18.2 nm, as shown in Figure 3c. This is in striking contrast with the obvious degradation tendency of Young's modulus for graphene and black phosphorus due to the interlayer slippage during the indentation,[43,44] suggesting relatively strong interlayer interactions for VS_2. Note that it has been pointed out that the point load assumption is effective only when the ratio of sample size to AFM tip radius (R_{tip}) is larger than 30.[45,46] To include such an indenter size effect in the analysis, Vella et al. introduced a prefactor of $\alpha \sim \left[1 - \left(\frac{R_{tip}}{r}\right)^{2/3}\right]^{-3}$ in the cubic term (δ^3).[47] In our case, $R_{tip} = 40$ nm and $r = 250-750$ nm, leading to an α value ranging from 1.08 to 1.20. Despite the subtle overestimation of Young's modulus here, the difference is within the margin of experimental error.

We note that VS_2 appears to be the softest among the 2D transition metal dichalcogenides (TMDs) library (Figure 3c). For instance, the Young's moduli are approximated to be 100 GPa for $MoTe_2$ and increase to ~170 GPa for $MoSe_2$ and WSe_2.[48−50] MoS_2 and WS_2 typically exhibit higher values ranging from 200 to 330 GPa.[19,42,51−53] Young's moduli of graphene and hBN can be even one magnitude larger than that of VS_2.[5,18,22,40,43,54−57] It is also found that the compliance of VS_2 is comparable to that of some main group metal chalcogenides, such as InSe, GaTe, and Bi_2Te_3.[58−60] As the Young's modulus reflects the change in elastic energy associated with the deformation of the atomic bonds, the softness of VS_2 can be hence explained by the relatively weaker V−S bonds compared to atomic bonding in other 2D materials. Particularly, while the V−S bond length (~2.36 Å) is similar to the Mo−S bond length (~2.31 Å), the larger V−S bond angle (~85.0°) in contrast to the Mo−S bond angle (~81.5°) enables VS_2 with a lower resistance to stretching (see more details in Tables S1 and S2).[33,61−63] In this regard, the excellent flexibility may endow VS_2 with mechanical advantages for the application in 2D material-based flexible electronics as it could offer high conformability as well as a minimal mismatch of mechanical property with soft substrates. Also, such compliance of VS_2 also enables high deformability when subjected to external loading, possibly benefiting the design of strain engineering.

As the load continuously increases to a critical level, a crack is induced and penetrates through the whole nanosheet across layers at the center, as shown in Figure S2. We found that the crack is localized and confined near the indenting tip. This was claimed to be ductile behaviors that could be traced back to a transition from intraplanar to interplanar fracture mechanism.[64,65] In this case, additional energy dissipation can confine the crack propagation, forming a localized fracture morphology. Based on the theory of linear elastic fracture mechanics, the fracture strength can be obtained by $\sigma_m^{2D} = \sqrt{F_m Et/4\pi R_{tip}}$, where F_m is breaking force and R_{tip} is the radius of spherical indenter.[18] For example, for a VS_2 nanosheet with $t = 9.2$ nm, $F_m = 2026.4$ nN and $R_{tip} = 40$ nm, rendering σ_m^{2D} to be 40.6 N/m. The corresponding three-dimensional (3D) fracture strength is summarized in Figure 4d, averaged as 4.6 ± 0.2 GPa. This is approximately one-tenth of the Young's modulus, agreeing well with the theoretical prediction of breaking strength of a defect-free material.[66]

Estimation of Bending Rigidity of VS_2. Though sometimes undesired in 2D materials, uniform buckles can be utilized for adhesion metrology between the 2D material and its substrate.[35,67] Here, instead, we extend this methodology to 2D VS_2 with nonuniform buckles and for the first time estimate its bending rigidity with a given adhesion energy. Figures 4a and 4b present SEM and AFM images of VS_2 nanosheets, showing relatively flat morphologies except for some tiny buckles at flake edges. Such buckled structures are perceived to originate from the vertical compression caused bending deformation of VS_2 nanosheets during the pressing process.

Figure 4c depicts the schematic of a VS_2 buckle that propagates through the sheet up to a finite distance L from the flake edge. AFM was employed to record the buckled morphology as well as successive cross-section profiles in x-coordinate. It is obvious that both buckle wavelength and amplitude increase over x. This nonuniform feature was previously reported for buckles formed by a thin polymeric film. Analogously, all buckle profiles take a cosine form[68]

$$z(y) = \frac{h}{2}\left(1 + \cos\frac{2\pi y}{w}\right) \quad (2)$$

where h and w are functions of x, standing for the amplitude and wavelength of the buckle, respectively. Similar to the polymeric case, the x-dependence of VS_2 buckle profiles disappears if the buckle profiles with y and z respectively normalized by $x^{1/3}$ and $x^{2/3}$ (Figure 4d and Figure S4). This implies that the formation of the buckle is a process to release the in-plane compressive strain completely. As a result, the bending energy becomes important that interacts with the adhesion energy between the sheet and the substrate.

In principle, the adhesion energy scales as $U_\gamma \sim \gamma$, and the bending energy (U_B) is proportional to Dh^2/w^4 where D is the bending rigidity.[69] At equilibrium, U_B should be of the same order with U_γ so as to give a characteristic length scale[70]

$$L_{ec} = \sqrt{\frac{D}{\gamma}} \sim \frac{w^2}{h} \quad (3)$$

https://dx.doi.org/10.1021/acsami.0c19835
ACS Appl. Mater. Interfaces 2021, 13, 3040−3050

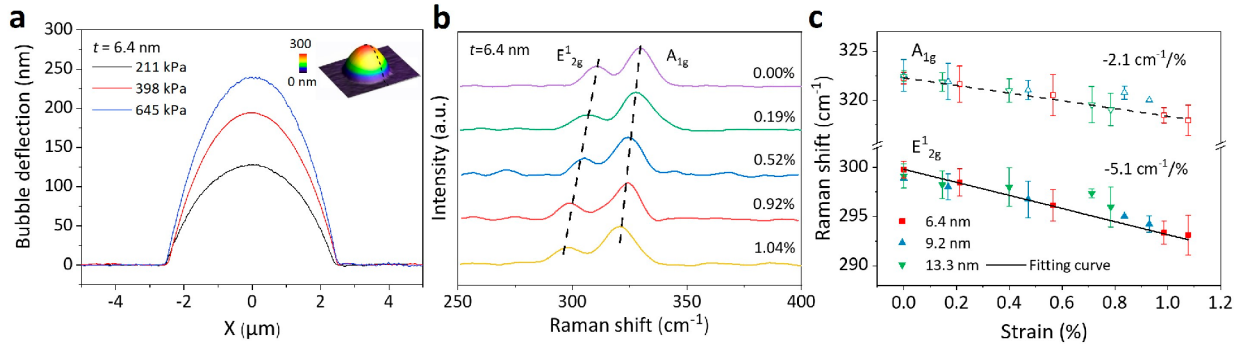

Figure 5. (a) AFM cross-section profiles of a bubble at various pressure differences, resulting in different biaxial strains at the center. The inset is the three-dimensional rendering of an AFM image showing the deformed shape of a VS_2 bubble at Δp = 645 kPa. (b) Raman spectra recorded at the bubble center with increasing bulging heights. (c) Peak positions for both E^1_{2g} and A_{1g} modes as a function of biaxial strain for different VS_2 thicknesses.

The elasto-capillary length (L_{ec}) is hence defined, which sets the curvature of the crest and accounts for the self-similarity of buckle profiles. Though the wavelength and amplitude of our buckles vary with the spatial location (x), they follow the $w \sim \sqrt{h}$ relation in eq 3 closely as shown in the inset of Figure 4e. However, samples with different thicknesses differ in the prefactor. We then normalized w and h by the elasto-capillary length and plotted them in a logarithmic scale in Figure 4e. By this way, normalized w and h of our samples with different thicknesses as well as measured at different locations can almost collapse to a master square-root relation, i.e., $w \sim \sqrt{hL_{ec}}$.

These observations indicate that for a given interfacial adhesion energy (γ) bending rigidity can be interpreted by the profiles of even nonuniform buckles in our work. Detailed analysis in the literature has provided the coefficient for the scaling relation in eq 3 such that[34,69]

$$D = \frac{\gamma w^4}{2\pi^4 h^2} \tag{4}$$

The bulge tests allow for the measurement of adhesion energy between VS_2 and SiO_2/Si substrate, yielding an average of 0.11 ± 0.03 J/m^2 (Figure S6), which agrees well with previous studies (0.082 − 0.170 J/m^2).[6,67] With the above-measured buckle amplitude and wavelength, the bending rigidity for VS_2 with various thicknesses can be deduced. In reality, such a proposed buckle-based approach shares the same mechanism with previously developed methods, wherein geometries of 2D materials such as folds and steps greatly rely on the adhesion energy.[9,71] Figure 4f shows the extracted bending rigidity of VS_2 nanosheets, which increases exponentially with their thickness, as expected. However, the scaling of $D \sim t^3$, due to classical plate theory, appears invalid and considerably overestimates the bending rigidity of the VS_2 multilayers. Specially, eight-layer VS_2 (~5.0 nm) displays a bending rigidity of ~4×10^{-16} N/m, which is enhanced to ~9×10^{-15} N/m as the thickness reaches ~15.5 nm, much lower than those (dashed line) expected from classical plate theory. Previous MD simulation concluded that interlayer coupling in multilayer graphene tends to mediate the load transfer between layers and the bending involves extension or compression of carbon bonds so that the plate phenomenology is fulfilled.[72] Such a conclusion has led to the wide use of $D_{the} = Et^3/12(1-\nu^2)$ for understanding the mechanics of out-of-plane deformations of multilayer 2D materials. Our results, however, show that interlayer coupling in VS_2 multilayers might be fairly weak, and the interlayer shear/sliding deformation could occur under even modest out-of-plane deformations, weakening the bending rigidity of the multilayer. This also points out the inappropriate use of classical plate assumption for multilayer 2D materials in the literature, where rich interlayer behaviors are overlooked.

To quantify the interlayer interaction between 2D materials, the spectroscopic technique and probe-based technique have been typically used.[73] For example, it has been demonstrated that Raman mapping of local strains allows the measurement of interlayer shear stress between bilayer graphene.[22,74] This method is only applicable to bilayer samples as the strain deconvolution becomes more complex for multilayers. However, exfoliation of thin VS_2 flakes (<5 nm) is highly challenging due to the limitation of the mechanical transfer of CVD grown bulk VS_2 crystals as well as the strong interlayer interactions between VS_2 layers. The probe-based friction test also affords an approach to determine the interlayer shear interactions, despite the difficulties in the attachment of 2D materials to the tips, which calls for more experimental efforts in the future.[75−77] In this scenario, here we defined a layer-dependent function $f(N) = D_{exp}/D_{the}$ to quantitatively describe the influence of interlayer coupling on bending rigidity of a N-layer 2D material (D_{exp} is the experimentally measured bending rigidity as summarized in Figure 4f). Theoretically, there are two limiting cases with which this calculation can be compared. The upper bound implies a perfectly bonded interface so that the interlayer slippage between adjacent layers is limited. The lower bound corresponds to frictionless interlayer interactions so that bending rigidity of a multilayer is the linear summation of the bending rigidity of a monolayer (Supporting Information S5). The calculated coefficients for the VS_2 multilayers sit between the two limits as depicted in Figure 4g, exhibiting a decreasing tendency with increasing thickness. Furthermore, the $f(N)$ values for VS_2 are relatively higher than that of MoS_2 across the thickness, implying stronger interlayer interactions mediated by interstitial V atoms between V−S layers. Our results are thus suggestive of the overestimated adhesion energy between multilayer MoS_2 and silicon substrate reported in the previous study, where the Young's modulus was adopted for calculation while neglecting the interlayer slippage.[67]

Determination of Grüneisen Parameter of VS_2. As discussed above, compared with other 2D materials, the high flexibility of VS_2 may benefit strain engineering applications—

https://dx.doi.org/10.1021/acsami.0c19835
ACS Appl. Mater. Interfaces 2021, 13, 3040−3050

using mechanical strain to tune their electronic properties. We here examine the Raman responses of VS_2 to biaxial strains. We transfer VS_2 sheets onto a cavity-patterned SiO_2/Si substrate and introduce the biaxial strain via pressurizing the sheets to bubbles. The bulging process was driven by the slow diffusion through the SiO_2 substrate to achieve a pressure difference across the sheet as previously reported.[22] We can measure the height and radius of the pressurized bubble by AFM, as shown in Figure 5a and Figure S5. The strain within the bubble reaches the maximum at the center, where we have equibiaxial tension with a magnitude of[78]

$$\varepsilon_{bi} = A(\upsilon)\left(\frac{H}{R}\right)^2 \tag{5}$$

where H is the bubble height, R is the bubble radius, and $A(\upsilon) = 2(3 - \upsilon)/5$ is a dimensionless function of Poisson's ratio (1.072 for $\upsilon = 0.32$). For instance, as a VS_2 nanosheet with t = 6.4 nm bulges up to ~250 nm while maintaining R = 2.5 μm, the center strain (ε_{bi}) could be around ~1%.

In fact, knowing the adhesion energy between VS_2 and SiO_2/Si substrate allows us to estimate the highest strain level attainable in the bubble at the critical pressure for the interfacial delamination (details can be seen in the Supporting Information, S4):[79]

$$\varepsilon_{max} = A(\upsilon)\sqrt{\frac{4\gamma C_2{}^3}{5C_1 Et}} \tag{6}$$

where C_1 and C_2 are constants dependent on the Poisson's ratio, which are 0.52 and 0.65 for VS_2, respectively. On the basis of our experimental results as presented above with E ~ 44.4 GPa, γ ~ 0.11 J/m^2, and t ~ 0.6 nm,[80] we could acquire the biaxial strain as high as ~6% for monolayers. Considering monolayers commonly conform more closely to the substrate than multilayers, resulting in even higher adhesion, the strain level could hence be further improved, opening up ample opportunities for the new physics and applications in VS_2 emerging at a high strain level.

Raman measurements were conducted to characterize the strain-engineered VS_2 sheet at the center of the bubble. Figure 5b shows a series of Raman spectra for VS_2 bubbles with different height-to-radius ratios. At the strain-free state ($H/A \approx 0$), the E^1_{2g} and A_{1g} peaks are located at 299.8 and 322.2 cm^{-1}, respectively. As the strain increases, we found clear softening behaviors for both modes. Even though the spatial resolution (~1 μm) is relatively large compared to the sample size (~5 μm), the peak shift can still be sensitive to the strain level and strain distribution within the laser spot because of the averaged effect of the collected Raman signal. After the peak shifts are plotted against the strains in Figure 5c, a linear dependence can be found with slopes of −5.1 and −2.1 cm^{-1}/% for E^1_{2g} and A_{1g} modes, respectively, regardless of the thickness. Under equibiaxial strain (ε_{bi}), the Raman band shifts ($\Delta\omega$) are related to the strain components through $\Delta\omega/\omega_0 = -2\varepsilon_{bi}\gamma$, where ω_0 and γ are the Raman peak position at zero strain and the Grüneisen parameter, respectively. Therefore, the Grüneisen parameters can be determined to be $\gamma_{E_{2g}{}^1} \approx 0.83$ and $\gamma_{A_{1g}} \approx 0.32$ for the first time for VS_2 sheets. Note that doping effects could be neglected since our results are based on the suspended system.[81]

CONCLUSIONS

In this work, we used three types of out-of-plane deformations of VS_2 sheets for their mechanical characterizations and strain engineering applications. Specifically, through poking the membrane that deforms like an inverse tent with AFM tips, the Young's modulus and fracture strength are obtained for samples with a variety of thicknesses. VS_2 is found to be the softest among the 2D TMD materials. Combining the morphology characterization with the adhesion energy between the 2D crystals and their substrates, bending rigidity is for the first time measured by a buckle-based method. Surprisingly, we uncovered that the classical plate model fails to account for the quantitative relationship between the Young's modulus and bending rigidity, which is possibly ascribed to the interlayer sliding. A microscale bubble offers an effective way to achieve uniform, controllable biaxial strains for continuously engineering the physics in 2D materials, based on which we realize the first measurement of the Grüneisen parameters for VS_2. Herein, our results may comprehensively elucidate the mechanical responses of VS_2 sheets that were not reported in the literature. Importantly, these quick yet effective techniques may be applied for the broad, emerging 2D materials, such as Mxene, metal/covalent organic frameworks (MOF/COF), and so forth.

METHODS

Fabrication and Characterization. The bulk vanadium disulfide (VS_2) samples were grown by the chemical vapor deposition (CVD) method under a mixed Ar/H_2 gas flow on the SiO_2/Si substrates at 600 °C, with solid VCl_3 and sulfur used as precursors. VS_2 nanosheets with various thicknesses were mechanically exfoliated from bulk materials and transferred onto another SiO_2/Si substrate. The lateral dimension and surface morphology were viewed by optical microscopy (Nikon LV100ND) and scanning electron microscopy (SEM, Hitachi S-4800, the acceleration voltage of 1−5 kV). An X-ray diffraction (XRD) (D/MAX-PC 2500) scan with a step size of 0.02° was employed to characterize the crystal structure of synthesized VS_2. Atomic force microscopy (AFM, Bruker Dimension Icon) was utilized to record the buckled structures via tapping mode. Raman spectroscopy (inVia-Renishaw) with an incident wavelength of 532 nm from a diode-pumped solid-state laser was employed to monitor the strain distribution within the VS_2 nanosheet. The spectral resolution is 1.0 cm^{-1}, and the spatial resolution is 1.0 μm. The laser intensity is kept below 0.5 mW to avoid the local heating-induced damage.

AFM Nanoindentation Test. An array of circular microwells was fabricated in a SiO_2/Si substrate by photolithography and reactive ion etching. The depth is ~1 μm, and the diameters range from 0.5 to 1.5 μm. VS_2 nanosheets were mechanically exfoliated and transferred onto such prepatterned substrates to form suspended systems. The nanoindentation test on the suspended graphene was performed in a commercial AFM system (Asylum Research, MFP-3D Infinity) by using AFM tips (NanoScience Instruments) with hemispherical geometry and low wear coating of tungsten carbide, and the nominal tip radius was ~40 nm.

Bulge Test. VS_2 sheets were transferred to a SiO_2/Si substrate and suspended over the microwells with a depth of ~300 nm and diameters of 5 μm. The samples were then placed into the pressure chamber to establish a pressure difference across the graphene membrane. Nitrogen gas was pumped into the chamber and gradually leaked into the cavities through the SiO_2/Si substrate until the internal pressure reaches that of the chamber ($p_{int} = p_0$). When removed from the chamber, the internal pressure would be higher than the atmospheric pressure (p_{ext}) outside so that the VS_2 membrane would bulge upward under such pressure difference

https://dx.doi.org/10.1021/acsami.0c19835
ACS Appl. Mater. Interfaces 2021, 13, 3040−3050

(Δp). The deflection (δ) and radius (r) of the bubble were measured by AFM tapping mode.

First-Principles Calculations. To calculate the Poisson's ratio and bending stiffness of monolayer VS_2 nanosheet, a density functional theory (DFT) calculation is performed via the Vienna *ab* initio simulation package (VASP).[82,83] The generalized gradient approximation (GGA) in the Perdew−Burke−Ernzerhof (PBE) form was used to describe the exchange-correlation functional,[84] and a cutoff energy of 500 eV for the plane-wave basis set was adopted. Projector augmented wave potentials were used for the ion−electron interactions.[85] Supercells consisting of 2 × 2 VS_2 unit cells are considered in the present calculations. A vacuum height of 15 Å in the z direction was adopted to avoid the interaction between two periodically repeated units. A k-point mesh with a density of about 40 Å (the product of each lattice constant and the corresponding number of k-points) was adopted for the Brillouin zone integration.[86] The structures were relaxed by using a conjugated-gradient algorithm. These settings were verified by an energy convergence threshold of 1 meV/atom and the threshold for force on atoms of 0.01 eV/Å. After the geometry is optimized, we calculated the Poisson's ratio in the direction of the armchair and zigzag via the equation

$$\nu = -(L_y - L_{y0})L_{x0}/(L_x - L_{x0})L_{y0} \quad (7)$$

where L_{x0} and L_{y0} are the initial lengths of VS_2 in the zigzag and armchair direction, respectively; at the same time L_x and L_y represent the deformed length. In the bending tests, we constructed a planar VS_2 ribbon and rolled it into a tube with a radius of R as used in our previous work.[87,88] Herein, periodic boundary conditions were used for the in-plane directions of VS_2 ribbon and axial direction of VS_2 tube, and additional vacuum layers of 20 Å were used in the other aperiodic directions. Afterward, the bending stiffness D can be calculated by using the relation $E^* = D/(2R^2)$, where E^* is the energy density difference between the ribbon and tube. To ensure the accuracy of the calculated D, tubes with different radius were used until the bending stiffness converges to 0.1 eV. Finally, the bending stiffness of VS_2 was calculated as 4.99 eV when a tube with radius 2.2 nm is used, considering a balance between computational accuracy and efficiency.

■ ASSOCIATED CONTENT

Supporting Information

The Supporting Information is available free of charge at https://pubs.acs.org/doi/10.1021/acsami.0c19835.

AFM nanoindentation; lattice parameter of VS_2; geometry of VS_2 buckles; bulge test; the function $f(N)$ in two limiting cases (PDF)

■ AUTHOR INFORMATION

Corresponding Authors

Luqi Liu − *CAS Key Laboratory of Nanosystem and Hierarchical Fabrication, CAS Center for Excellence in Nanoscience, National Center for Nanoscience and Technology, Beijing 100190, P. R. China;* orcid.org/0000-0002-5752-1638; Email: liulq@nanoctr.cn

Zhong Zhang − *CAS Key Laboratory of Nanosystem and Hierarchical Fabrication, CAS Center for Excellence in Nanoscience, National Center for Nanoscience and Technology, Beijing 100190, P. R. China;* orcid.org/0000-0002-9102-1311; Email: zhong.zhang@nanoctr.cn

Authors

Guorui Wang − *CAS Key Laboratory of Nanosystem and Hierarchical Fabrication, CAS Center for Excellence in Nanoscience, National Center for Nanoscience and Technology, Beijing 100190, P. R. China; Department of Mechanical and Industrial Engineering, University of Toronto, Toronto, Ontario M5S 3G8, Canada;* orcid.org/0000-0002-1746-3410

Zhepeng Zhang − *Department of Materials Science and Engineering, College of Engineering, Peking University, Beijing 100871, P. R. China;* orcid.org/0000-0002-9870-0720

Yanlei Wang − *State Key Laboratory of Multiphase Complex Systems, Beijing Key Laboratory of Ionic Liquids Clean Process, Institute of Process Engineering, Chinese Academy of Sciences, Beijing 100190, P. R. China;* orcid.org/0000-0002-2214-8781

Enlai Gao − *Department of Engineering Mechanics, School of Civil Engineering, Wuhan University, Wuhan, Hubei 430072, P. R. China;* orcid.org/0000-0003-1960-0260

Xiangzheng Jia − *Department of Engineering Mechanics, School of Civil Engineering, Wuhan University, Wuhan, Hubei 430072, P. R. China*

Zhaohe Dai − *CAS Key Laboratory of Nanosystem and Hierarchical Fabrication, CAS Center for Excellence in Nanoscience, National Center for Nanoscience and Technology, Beijing 100190, P. R. China;* orcid.org/0000-0002-5205-089X

Chuanxin Weng − *CAS Key Laboratory of Nanosystem and Hierarchical Fabrication, CAS Center for Excellence in Nanoscience, National Center for Nanoscience and Technology, Beijing 100190, P. R. China*

Yanfeng Zhang − *Department of Materials Science and Engineering, College of Engineering, Peking University, Beijing 100871, P. R. China;* orcid.org/0000-0003-1319-3270

Complete contact information is available at: https://pubs.acs.org/10.1021/acsami.0c19835

Notes

The authors declare no competing financial interest.

■ ACKNOWLEDGMENTS

This work was jointly supported by National Natural Science Foundation of China (Grants 11832010, 11890682, 22072031, and 21721002), the Strategic Priority Research Program of Chinese Academy of Sciences (CAS) under Grants XDB30020100, the National Key Research and Development Program under Grant 2018YFA0208403, and the National Key Basic Research Program of China (Grant 2013CB934203).

■ REFERENCES

(1) Zang, J.; Ryu, S.; Pugno, N.; Wang, Q.; Tu, Q.; Buehler, M. J.; Zhao, X. Multifunctionality and Control of the Crumpling and Unfolding of Large-Area Graphene. *Nat. Mater.* **2013**, *12*, 321−325.

(2) Deng, S.; Berry, V. Wrinkled, Rippled and Crumpled Graphene: An Overview of Formation Mechanism, Electronic Properties, and Applications. *Mater. Today* **2016**, *19*, 197−212.

(3) Castellanos-Gomez, A.; Roldan, R.; Cappelluti, E.; Buscema, M.; Guinea, F.; van der Zant, H. S.; Steele, G. A. Local Strain Engineering in Atomically Thin MoS_2. *Nano Lett.* **2013**, *13*, 5361−5366.

(4) Yang, S.; Wang, C.; Sahin, H.; Chen, H.; Li, Y.; Li, S. S.; Suslu, A.; Peeters, F. M.; Liu, Q.; Li, J.; Tongay, S. Tuning the Optical, Magnetic, and Electrical Properties of $ReSe_2$ by Nanoscale Strain Engineering. *Nano Lett.* **2015**, *15*, 1660−1666.

(5) Koenig, S. P.; Boddeti, N. G.; Dunn, M. L.; Bunch, J. S. Ultrastrong Adhesion of Graphene Membranes. *Nat. Nanotechnol.* **2011**, *6*, 543−546.

(6) Sanchez, D. A.; Dai, Z.; Wang, P.; Cantu-Chavez, A.; Brennan, C. J.; Huang, R.; Lu, N. Mechanics of Spontaneously Formed Nanoblisters Trapped by Transferred 2D Crystals. *Proc. Natl. Acad. Sci. U. S. A.* **2018**, *115*, 7884−7889.

(7) Jiang, Y.; Mao, J.; Duan, J.; Lai, X.; Watanabe, K.; Taniguchi, T.; Andrei, E. Y. Visualizing Strain-Induced Pseudomagnetic Fields in Graphene through an hBN Magnifying Glass. *Nano Lett.* **2017**, *17*, 2839−2843.
(8) Dai, Z.; Hou, Y.; Sanchez, D. A.; Wang, G.; Brennan, C. J.; Zhang, Z.; Liu, L.; Lu, N. Interface-Governed Deformation of Nanobubbles and Nanotents Formed by Two-Dimensional Materials. *Phys. Rev. Lett.* **2018**, *121*, 266101.
(9) Zhao, J.; Deng, Q.; Ly, T. H.; Han, G. H.; Sandeep, G.; Rummeli, M. H. Two-Dimensional Membrane as Elastic Shell with Proof on the Folds Revealed by Three-Dimensional Atomic Mapping. *Nat. Commun.* **2015**, *6*, 8935−8940.
(10) Annett, J.; Cross, G. L. Self-Assembly of Graphene Ribbons by Spontaneous Self-Tearing and Peeling from a Substrate. *Nature* **2016**, *535*, 271−275.
(11) Xu, Z.; Buehler, M. J. Geometry Controls Conformation of Graphene Sheets: Membranes, Ribbons, and Scrolls. *ACS Nano* **2010**, *4*, 3869−3876.
(12) Cui, X.; Kong, Z.; Gao, E.; Huang, D.; Hao, Y.; Shen, H.; Di, C. A.; Xu, Z.; Zheng, J.; Zhu, D. Rolling up Transition Metal Dichalcogenide Nanoscrolls Via One Drop of Ethanol. *Nat. Commun.* **2018**, *9*, 1301−1307.
(13) Wang, M. C.; Leem, J.; Kang, P.; Choi, J.; Knapp, P.; Yong, K.; Nam, S. Mechanical Instability Driven Self-Assembly and Architecturing of 2D Materials. *2D Mater.* **2017**, *4*, 022002.
(14) Kinloch, I. A.; Suhr, J.; Lou, J.; Young, R. J.; Ajayan, P. M. Composites with Carbon Nanotubes and Graphene: An Outlook. *Science* **2018**, *362*, 547−553.
(15) Wang, G.; Liu, L.; Zhang, Z. Interface Mechanics in Carbon Nanomaterials-Based Nanocomposites. *Composites, Part A* **2021**, *141*, 106212.
(16) Deng, S.; Sumant, A. V.; Berry, V. Strain Engineering in Two-Dimensional Nanomaterials Beyond Graphene. *Nano Today* **2018**, *22*, 14−35.
(17) Dai, Z.; Liu, L.; Zhang, Z. Strain Engineering of 2D Materials: Issues and Opportunities at the Interface. *Adv. Mater.* **2019**, *31*, 1805417.
(18) Lee, C.; Wei, X.; Kysar, J. W.; Hone, J. Measurement of the Elastic Properties and Intrinsic Strength of Monolayer Graphene. *Science* **2008**, *321*, 385−388.
(19) Bertolazzi, S.; Brivio, J.; Kis, A. Stretching and Breaking of Ultrathin MoS_2. *ACS Nano* **2011**, *5*, 9703−9709.
(20) Lipatov, A.; Lu, H. D.; Alhabeb, M.; Anasori, B.; Gruverman, A.; Gogotsi, Y.; Sinitskii, A. Elastic Properties of 2D $Ti_3C_2T_x$Mxene Monolayers and Bilayers. *Sci. Adv.* **2018**, *4*, No. eaat0491.
(21) Wang, G.; Li, X.; Wang, Y.; Zheng, Z.; Dai, Z.; Qi, X.; Liu, L.; Cheng, Z.; Xu, Z.; Tan, P.; Zhang, Z. Interlayer Coupling Behaviors of Boron Doped Multilayer Graphene. *J. Phys. Chem. C* **2017**, *121*, 26034−26043.
(22) Wang, G.; Dai, Z.; Wang, Y.; Tan, P.; Liu, L.; Xu, Z.; Wei, Y.; Huang, R.; Zhang, Z. Measuring Interlayer Shear Stress in Bilayer Graphene. *Phys. Rev. Lett.* **2017**, *119*, 036101.
(23) Wang, G.; Dai, Z.; Xiao, J.; Feng, S.; Weng, C.; Liu, L.; Xu, Z.; Huang, R.; Zhang, Z. Bending of Multilayer van der Waals Materials. *Phys. Rev. Lett.* **2019**, *123*, 116101.
(24) Ma, Y.; Wang, G.; Chen, Y.; Long, D.; Guan, Y.; Liu, L.; Zhang, Z. Extended Hencky Solution for the Blister Test of Nanomembrane. *Extrem. Mech. Lett.* **2018**, *22*, 69−78.
(25) Bao, W.; Miao, F.; Chen, Z.; Zhang, H.; Jang, W.; Dames, C.; Lau, C. N. Controlled Ripple Texturing of Suspended Graphene and Ultrathin Graphite Membranes. *Nat. Nanotechnol.* **2009**, *4*, 562−566.
(26) Ji, Q.; Li, C.; Wang, J.; Niu, J.; Gong, Y.; Zhang, Z.; Fang, Q.; Zhang, Y.; Shi, J.; Liao, L.; Wu, X.; Gu, L.; Liu, Z.; Zhang, Y. Metallic Vanadium Disulfide Nanosheets as a Platform Material for Multifunctional Electrode Applications. *Nano Lett.* **2017**, *17*, 4908−4916.
(27) Yuan, J.; Wu, J.; Hardy, W. J.; Loya, P.; Lou, M.; Yang, Y.; Najmaei, S.; Jiang, M.; Qin, F.; Keyshar, K.; Ji, H.; Gao, W.; Bao, J.; Kono, J.; Natelson, D.; Ajayan, P. M.; Lou, J. Facile Synthesis of Single Crystal Vanadium Disulfide Nanosheets by Chemical Vapor Deposition for Efficient Hydrogen Evolution Reaction. *Adv. Mater.* **2015**, *27*, 5605−5609.
(28) Gao, D.; Xue, Q.; Mao, X.; Wang, W.; Xu, Q.; Xue, D. Ferromagnetism in Ultrathin VS_2 Nanosheets. *J. Mater. Chem. C* **2013**, *1*, 5909−5916.
(29) Arnold, F.; Stan, R.-M.; Mahatha, S. K.; Lund, H. E.; Curcio, D.; Dendzik, M.; Bana, H.; Travaglia, E.; Bignardi, L.; Lacovig, P.; Lizzit, D.; Li, Z.; Bianchi, M.; Miwa, J. A.; Bremholm, M.; Lizzit, S.; Hofmann, P.; Sanders, C. E. Novel Single-Layer Vanadium Sulphide Phases. *2D Mater.* **2018**, *5*, 045009.
(30) Ma, Y.; Dai, Y.; Guo, M.; Niu, C.; Zhu, Y.; Huang, B. Evidence of the Existence of Magnetism in Pristine VX_2 Monolayers (X = S, Se) and Their Strain-Induced Tunable Magnetic Properties. *ACS Nano* **2012**, *6*, 1695−1701.
(31) Kan, M.; Wang, B.; Lee, Y. H.; Sun, Q. A Density Functional Theory Study of the Tunable Structure, Magnetism and Metal-Insulator Phase Transition in VS_2 Monolayers Induced by in-Plane Biaxial Strain. *Nano Res.* **2015**, *8*, 1348−1356.
(32) Feng, J.; Peng, L.; Wu, C.; Sun, X.; Hu, S.; Lin, C.; Dai, J.; Yang, J.; Xie, Y. Giant Moisture Responsiveness of VS_2 Ultrathin Nanosheets for Novel Touchless Positioning Interface. *Adv. Mater.* **2012**, *24*, 1969−1974.
(33) Jing, Y.; Zhou, Z.; Cabrera, C. R.; Chen, Z. Metallic VS_2 Monolayer: A Promising 2D Anode Material for Lithium Ion Batteries. *J. Phys. Chem. C* **2013**, *117*, 25409−25413.
(34) Brennan, C. J.; Nguyen, J.; Yu, E. T.; Lu, N. S. Interface Adhesion between 2D Materials and Elastomers Measured by Buckle Delaminations. *Adv. Mater. Interfaces* **2015**, *2*, 1500176.
(35) Iguiniz, N.; Frisenda, R.; Bratschitsch, R.; Castellanos-Gomez, A. Revisiting the Buckling Metrology Method to Determine the Young's Modulus of 2D Materials. *Adv. Mater.* **2019**, *31*, 1807150.
(36) He, P.; Yan, M.; Zhang, G.; Sun, R.; Chen, L.; An, Q.; Mai, L. Layered VS_2 Nanosheet-Based Aqueous Zn Ion Battery Cathode. *Adv. Energy Mater.* **2017**, *7*, 1601920.
(37) Littlejohn, A. J.; Li, Z.; Lu, Z.; Sun, X.; Nawarat, P.; Wang, Y.; Li, Y.; Wang, T.; Chen, Y.; Zhang, L.; Li, H.; Kisslinger, K.; Shi, S.; Shi, J.; Raeliarijaona, A.; Shi, W.; Terrones, H.; Lewis, K. M.; Washington, M.; Lu, T.-M.; Wang, G.-C. Large Metallic Vanadium Disulfide Ultrathin Flakes for Spintronic Circuits and Quantum Computing Devices. *ACS Appl. Nano Mater.* **2019**, *2*, 3684−3694.
(38) Zhang, J.; Zhang, C.; Wang, Z.; Zhu, J.; Wen, Z.; Zhao, X.; Zhang, X.; Xu, J.; Lu, Z. Synergistic Interlayer and Defect Engineering in VS_2 Nanosheets toward Efficient Electrocatalytic Hydrogen Evolution Reaction. *Small* **2018**, *14*, 1703098.
(39) Hossain, M.; Wu, J.; Wen, W.; Liu, H.; Wang, X.; Xie, L. Chemical Vapor Deposition of 2D Vanadium Disulfide and Diselenide and Raman Characterization of the Phase Transitions. *Adv. Mater. Interfaces* **2018**, *5*, 1800528.
(40) Dai, Z.; Wang, G.; Zheng, Z.; Wang, Y.; Zhang, S.; Qi, X.; Tan, P.; Liu, L.; Xu, Z.; Li, Q.; Cheng, Z.; Zhang, Z. Mechanical Responses of Boron-Doped Monolayer Graphene. *Carbon* **2019**, *147*, 594−601.
(41) Komaragiri, U.; Begley, M. R.; Simmonds, J. G. The Mechanical Response of Freestanding Circular Elastic Films under Point and Pressure Loads. *J. Appl. Mech.* **2005**, *72*, 203−212.
(42) Castellanos-Gomez, A.; Poot, M.; Steele, G. A.; van der Zant, H. S.; Agrait, N.; Rubio-Bollinger, G. Elastic Properties of Freely Suspended MoS_2 Nanosheets. *Adv. Mater.* **2012**, *24*, 772−5.
(43) Falin, A.; Cai, Q.; Santos, E. J. G.; Scullion, D.; Qian, D.; Zhang, R.; Yang, Z.; Huang, S.; Watanabe, K.; Taniguchi, T.; Barnett, M. R.; Chen, Y.; Ruoff, R. S.; Li, L. H. Mechanical Properties of Atomically Thin Boron Nitride and the Role of Interlayer Interactions. *Nat. Commun.* **2017**, *8*, 15815−15813.
(44) Wang, J. Y.; Li, Y.; Zhan, Z. Y.; Li, T.; Zhen, L.; Xu, C. Y. Elastic Properties of Suspended Black Phosphorus Nanosheets. *Appl. Phys. Lett.* **2016**, *108*, 013104.
(45) Begley, M. R.; Mackin, T. J. Spherical Indentation of Freestanding Circular Thin Films in the Membrane Regime. *J. Mech. Phys. Solids* **2004**, *52*, 2005−2023.

https://dx.doi.org/10.1021/acsami.0c19835
ACS Appl. Mater. Interfaces 2021, 13, 3040−3050

(46) Cao, G.; Gao, H. Mechanical Properties Characterization of Two-Dimensional Materials Via Nanoindentation Experiments. *Prog. Mater. Sci.* **2019**, *103*, 558−595.
(47) Vella, D.; Davidovitch, B. Indentation Metrology of Clamped, Ultra-Thin Elastic Sheets. *Soft Matter* **2017**, *13*, 2264−2278.
(48) Yang, Y.; Li, X.; Wen, M.; Hacopian, E.; Chen, W.; Gong, Y.; Zhang, J.; Li, B.; Zhou, W.; Ajayan, P. M.; Chen, Q.; Zhu, T.; Lou, J. Brittle Fracture of 2D $MoSe_2$. *Adv. Mater.* **2017**, *29*, 1604201.
(49) Zhang, R.; Koutsos, V.; Cheung, R. Elastic Properties of Suspended Multilayer WSe_2. *Appl. Phys. Lett.* **2016**, *108*, 042104.
(50) Sun, Y.; Pan, J.; Zhang, Z.; Zhang, K.; Liang, J.; Wang, W.; Yuan, Z.; Hao, Y.; Wang, B.; Wang, J.; Wu, Y.; Zheng, J.; Jiao, L.; Zhou, S.; Liu, K.; Cheng, C.; Duan, W.; Xu, Y.; Yan, Q.; Liu, K. Elastic Properties and Fracture Behaviors of Biaxially Deformed, Polymorphic $MoTe_2$. *Nano Lett.* **2019**, *19*, 761−769.
(51) Lloyd, D.; Liu, X.; Boddeti, N.; Cantley, L.; Long, R.; Dunn, M. L.; Bunch, J. S. Adhesion, Stiffness, and Instability in Atomically Thin MoS_2 Bubbles. *Nano Lett.* **2017**, *17*, 5329−5334.
(52) Cooper, R. C.; Lee, C.; Marianetti, C. A.; Wei, X.; Hone, J.; Kysar, J. W. Nonlinear Elastic Behavior of Two-Dimensional Molybdenum Disulfide. *Phys. Rev. B: Condens. Matter Mater. Phys.* **2013**, *87*, 035423.
(53) Liu, K.; Yan, Q.; Chen, M.; Fan, W.; Sun, Y.; Suh, J.; Fu, D.; Lee, S.; Zhou, J.; Tongay, S.; Ji, J.; Neaton, J. B.; Wu, J. Elastic Properties of Chemical-Vapor-Deposited Monolayer MoS_2, WS_2, and Their Bilayer Heterostructures. *Nano Lett.* **2014**, *14*, 5097−5103.
(54) Song, L.; Ci, L.; Lu, H.; Sorokin, P. B.; Jin, C.; Ni, J.; Kvashnin, A. G.; Kvashnin, D. G.; Lou, J.; Yakobson, B. I.; Ajayan, P. M. Large Scale Growth and Characterization of Atomic Hexagonal Boron Nitride Layers. *Nano Lett.* **2010**, *10*, 3209−3215.
(55) Kim, S. M.; Hsu, A.; Park, M. H.; Chae, S. H.; Yun, S. J.; Lee, J. S.; Cho, D. H.; Fang, W.; Lee, C.; Palacios, T.; Dresselhaus, M.; Kim, K. K.; Lee, Y. H.; Kong, J. Synthesis of Large-Area Multilayer Hexagonal Boron Nitride for High Material Performance. *Nat. Commun.* **2015**, *6*, 8662−8672.
(56) Cao, K.; Feng, S.; Han, Y.; Gao, L.; Hue Ly, T.; Xu, Z.; Lu, Y. Elastic Straining of Free-Standing Monolayer Graphene. *Nat. Commun.* **2020**, *11*, 284.
(57) Han, Y.; Feng, S.; Cao, K.; Wang, Y.; Gao, L.; Xu, Z.; Lu, Y. Large Elastic Deformation and Defect Tolerance of Hexagonal Boron Nitride Monolayers. *Cell Rep. Phys. Sci.* **2020**, *1*, 100172.
(58) Li, Y.; Yu, C.; Gan, Y.; Kong, Y.; Jiang, P.; Zou, D. F.; Li, P.; Yu, X. F.; Wu, R.; Zhao, H.; Gao, C. F.; Li, J. Elastic Properties and Intrinsic Strength of Two-Dimensional InSe Flakes. *Nanotechnology* **2019**, *30*, 335703.
(59) Chitara, B.; Ya'akobovitz, A. Elastic Properties and Breaking Strengths of GaS, GaSe and GaTe Nanosheets. *Nanoscale* **2018**, *10*, 13022−13027.
(60) Guo, L.; Yan, H.; Moore, Q.; Buettner, M.; Song, J.; Li, L.; Araujo, P. T.; Wang, H. T. Elastic Properties of van der Waals Epitaxy Grown Bismuth Telluride 2D Nanosheets. *Nanoscale* **2015**, *7*, 11915−11921.
(61) Li, J.; Medhekar, N. V.; Shenoy, V. B. Bonding Charge Density and Ultimate Strength of Monolayer Transition Metal Dichalcogenides. *J. Phys. Chem. C* **2013**, *117*, 15842−15848.
(62) Kanoun, M. B.; Goumri-Said, S. Tailoring Optoelectronic Properties of Monolayer Transition Metal Dichalcogenide through Alloying. *Materialia* **2020**, *12*, 100708.
(63) Wang, W.; Sun, Z.; Zhang, W.; Fan, Q.; Sun, Q.; Cui, X.; Xiang, B. First-Principles Investigations of Vanadium Disulfide for Lithium and Sodium Ion Battery Applications. *RSC Adv.* **2016**, *6*, 54874−54879.
(64) Cao, C.; Daly, M.; Chen, B.; Howe, J. Y.; Singh, C. V.; Filleter, T.; Sun, Y. Strengthening in Graphene Oxide Nanosheets: Bridging the Gap between Interplanar and Intraplanar Fracture. *Nano Lett.* **2015**, *15*, 6528−34.
(65) Li, P.; Jiang, C.; Xu, S.; Zhuang, Y.; Gao, L.; Hu, A.; Wang, H.; Lu, Y. In Situ Nanomechanical Characterization of Multi-Layer MoS_2 Membranes: From Intraplanar to Interplanar Fracture. *Nanoscale* **2017**, *9*, 9119−9128.
(66) Felbeck, D. K.; Atkins, A. G. *Strength and Fracture of Engineering Solids*; Prentice-Hall: Englewood Cliffs, NJ, 1984.
(67) Deng, S.; Gao, E.; Xu, Z.; Berry, V. Adhesion Energy of MoS_2 Thin Films on Silicon-Based Substrates Determined Via the Attributes of a Single MoS_2 Wrinkle. *ACS Appl. Mater. Interfaces* **2017**, *9*, 7812−7818.
(68) Dai, Z.; Sanchez, D. A.; Brennan, C. J.; Lu, N. Radial Buckle Delamination around 2D Material Tents. *J. Mech. Phys. Solids* **2020**, *137*, 103843.
(69) Vella, D.; Bico, J.; Boudaoud, A.; Roman, B.; Reis, P. M. The Macroscopic Delamination of Thin Films from Elastic Substrates. *Proc. Natl. Acad. Sci. U. S. A.* **2009**, *106*, 10901−10906.
(70) Roman, B.; Bico, J. Elasto-Capillarity: Deforming an Elastic Structure with a Liquid Droplet. *J. Phys.: Condens. Matter* **2010**, *22*, 493101.
(71) Han, E.; Yu, J.; Annevelink, E.; Son, J.; Kang, D. A.; Watanabe, K.; Taniguchi, T.; Ertekin, E.; Huang, P. Y.; van der Zande, A. M. Ultrasoft Slip-Mediated Bending in Few-Layer Graphene. *Nat. Mater.* **2020**, *19*, 305−309.
(72) Zhang, D. B.; Akatyeva, E.; Dumitrica, T. Bending Ultrathin Graphene at the Margins of Continuum Mechanics. *Phys. Rev. Lett.* **2011**, *106*, 255503.
(73) Dai, Z.; Lu, N.; Liechti, K. M.; Huang, R. Mechanics at the Interfaces of 2D Materials: Challenges and Opportunities. *Curr. Opin. Solid State Mater. Sci.* **2020**, *24*, 100837.
(74) Androulidakis, C.; Koukaras, E. N.; Paterakis, G.; Trakakis, G.; Galiotis, C. Tunable Macroscale Structural Superlubricity in Two-Layer Graphene Via Strain Engineering. *Nat. Commun.* **2020**, *11*, 1−11.
(75) Liu, S. W.; Wang, H. P.; Xu, Q.; Ma, T. B.; Yu, G.; Zhang, C.; Geng, D.; Yu, Z.; Zhang, S.; Wang, W.; Hu, Y. Z.; Wang, H.; Luo, J. Robust Microscale Superlubricity under High Contact Pressure Enabled by Graphene-Coated Microsphere. *Nat. Commun.* **2017**, *8*, 14029.
(76) Liu, Y.; Song, A.; Xu, Z.; Zong, R.; Zhang, J.; Yang, W.; Wang, R.; Hu, Y.; Luo, J.; Ma, T. Interlayer Friction and Superlubricity in Single-Crystalline Contact Enabled by Two-Dimensional Flake-Wrapped Atomic Force Microscope Tips. *ACS Nano* **2018**, *12*, 7638−7646.
(77) Li, H.; Wang, J.; Gao, S.; Chen, Q.; Peng, L.; Liu, K.; Wei, X. Superlubricity between MoS_2 Monolayers. *Adv. Mater.* **2017**, *29*, 1701474−1701479.
(78) Wang, P.; Gao, W.; Cao, Z.; Liechti, K. M.; Huang, R. Numerical Analysis of Circular Graphene Bubbles. *J. Appl. Mech.* **2013**, *80*, 040905.
(79) Boddeti, N. G.; Koenig, S. P.; Long, R.; Xiao, J.; Bunch, J. S.; Dunn, M. L. Mechanics of Adhered, Pressurized Graphene Blisters. *J. Appl. Mech.* **2013**, *80*, 040909.
(80) Su, J.; Wang, M.; Li, Y.; Wang, F.; Chen, Q.; Luo, P.; Han, J.; Wang, S.; Li, H.; Zhai, T. Sub-Millimeter Scale Monolayer p-type H-Phase VS_2. *Adv. Funct. Mater.* **2020**, *30*, 2000240.
(81) Lee, J. E.; Ahn, G.; Shim, J.; Lee, Y. S.; Ryu, S. Optical Separation of Mechanical Strain from Charge Doping in Graphene. *Nat. Commun.* **2012**, *3*, 1024.
(82) Kresse, G.; Furthmüller, J. Efficient Iterative Schemes for Ab Initio Total-Energy Calculations Using a Plane-Wave Basis Set. *Phys. Rev. B: Condens. Matter Mater. Phys.* **1996**, *54*, 11169.
(83) Kresse, G.; Furthmuller, J. Efficiency of Ab-initio Total Energy Calculations for Metals and Semiconductors Using a Plane-Wave Basis Set. *Comput. Mater. Sci.* **1996**, *6*, 15−50.
(84) Perdew, J. P.; Burke, K.; Ernzerhof, M. Generalized Gradient Approximation Made Simple. *Phys. Rev. Lett.* **1996**, *77*, 3865−3868.
(85) Blochl, P. E. Projector Augmented-Wave Method. *Phys. Rev. B: Condens. Matter Mater. Phys.* **1994**, *50*, 17953−17979.
(86) Monkhorst, H. J.; Pack, J. D. Special Points for Brillouin-Zone Integrations. *Phys. Rev. B* **1976**, *13*, 5188.

https://dx.doi.org/10.1021/acsami.0c19835
ACS Appl. Mater. Interfaces 2021, 13, 3040−3050

(87) Gao, E.; Lin, S.-Z.; Qin, Z.; Buehler, M. J.; Feng, X.-Q.; Xu, Z. Mechanical Exfoliation of Two-Dimensional Materials. *J. Mech. Phys. Solids* **2018**, *115*, 248−262.
(88) Gao, E. L.; Xu, Z. P. Thin-Shell Thickness of Two-Dimensional Materials. *J. Appl. Mech.* **2015**, *82*, 121012.

https://dx.doi.org/10.1021/acsami.0c19835
ACS Appl. Mater. Interfaces 2021, 13, 3040−3050

Supporting Information

Out-of-Plane Deformations Determined Mechanics of Vanadium Disulfide (VS_2) Sheets

Guorui Wang[1, 5], Zhepeng Zhang[2], Yanlei Wang[3], Enlai Gao[4], Xiangzheng Jia[4], Zhaohe Dai[1], Chuanxin Weng[1], Luqi Liu[1,*], Yanfeng Zhang[2], Zhong Zhang[1,*]

[1]CAS Key Laboratory of Nanosystem and Hierarchical Fabrication, CAS Center for Excellence in Nanoscience, National Center for Nanoscience and Technology, Beijing, 100190, P.R. China

[2]Department of Materials Science and Engineering, College of Engineering, Peking University, Beijing 100871, People's Republic of China

[3]State Key Laboratory of Multiphase Complex Systems, Beijing Key Laboratory of Ionic Liquids Clean Process, Institute of Process Engineering, Chinese Academy of Sciences, Beijing 100190, China

[4]Department of Engineering Mechanics, School of Civil Engineering, Wuhan University, Wuhan, Hubei 430072, China

[5]Department of Mechanical and Industrial Engineering, University of Toronto, 5 King's College Road, Toronto, Ontario M5S 3G8, Canada

Correspondence and requests for materials should be addressed to L.L. (email: liulq@nanoctr.cn) or to Z.Z. (email: zhong.zhang@nanoctr.cn).

S1. AFM nanoindentation

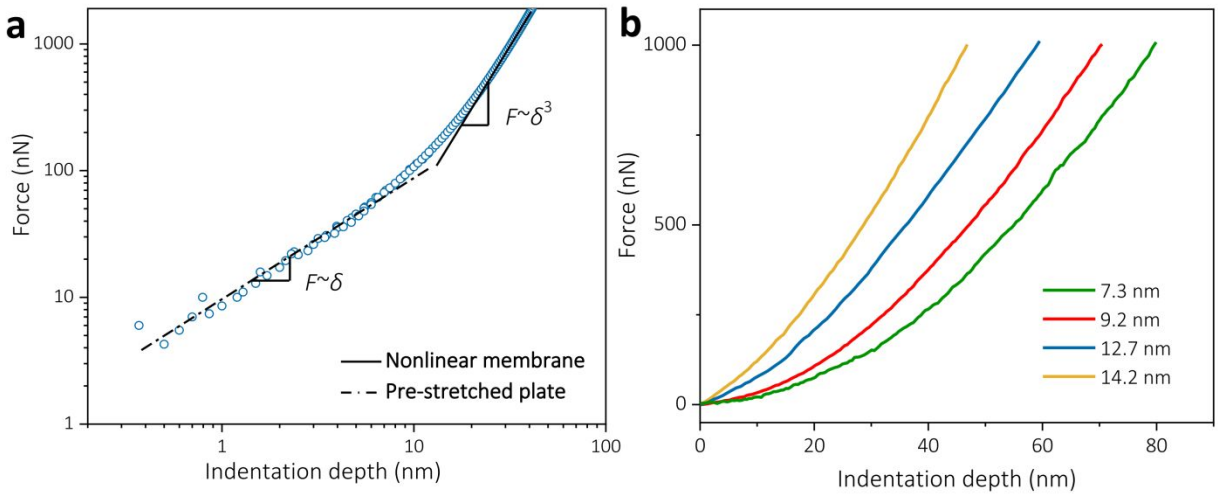

Figure S1. (a) Force-indentation depth curve plotted in logarithmic coordinates, where a linear relationship can be observed in the first stage dominated by pre-tension and bending rigidity, while it gradually becomes a cubic relationship as the force increases with membrane characteristics. (b) Representative force-indentation depth curves for suspended VS_2 nanosheets with different thicknesses.

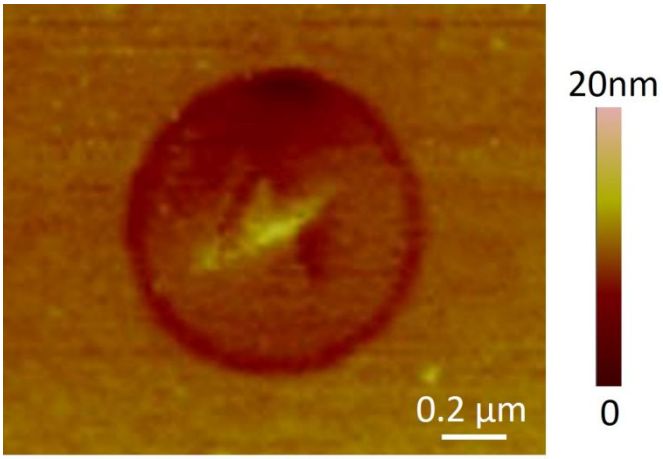

Figure S2. The fracture morphology of VS_2 nanosheet after the nanoindentation test, where a localized crack can be observed.

S2. Lattice parameter of VS_2

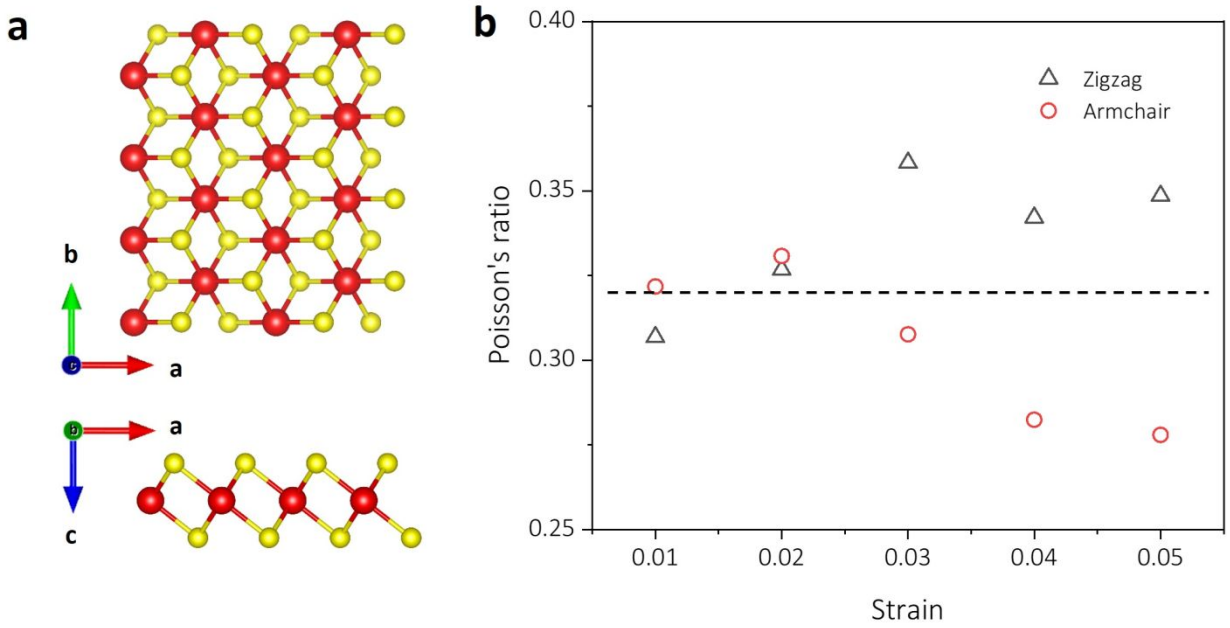

Figure S3. (a) Schematic of atomic configuration of 1T VS_2 used in DFT calculation, where the red atom is vanadium (V) and the yellow atom is sulfur (S). (b) The strain − Poisson's ratio curve of VS_2 in the direction of armchair and zigzag.

Table S1. Parameters for the atomic configuration of VS_2.

$d_{V\text{-}V}$ (Å)	$d_{V\text{-}S}$ (Å)	$Angle_{V\text{-}S\text{-}V}$ (°)	*a* (Å)	*b* (Å)
3.1609	2.35	84.4245	3.1609	5.47087

Table S2. Atomic bond length and angle for different 2D transition metal dichalcogenides materials.

Materials	Bond length (Å)	Bond angle (°)	Ref.
MoS_2	2.31	81.49	[1, 2]
$MoSe_2$	2.51	82.56	[1, 3]
$MoTe_2$	2.70	81.00	[1, 2]
WS_2	2.39	80.80	[1, 4]
VS_2	2.36	84.43 - 85.06	[5, 6]

S3. Geometry of VS_2 buckles

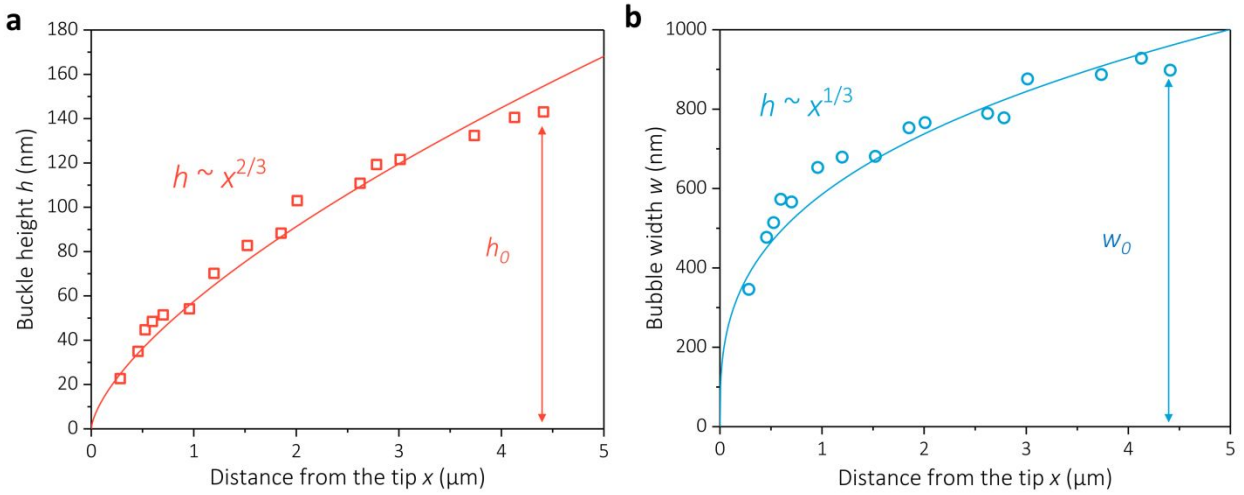

Figure S4. (a) Buckle height and (b) width as a function of the distance from the tip (x). The experimental data are fitted by power functions with 2/3 and 1/3 exponents, respectively.

S4. Bulge test

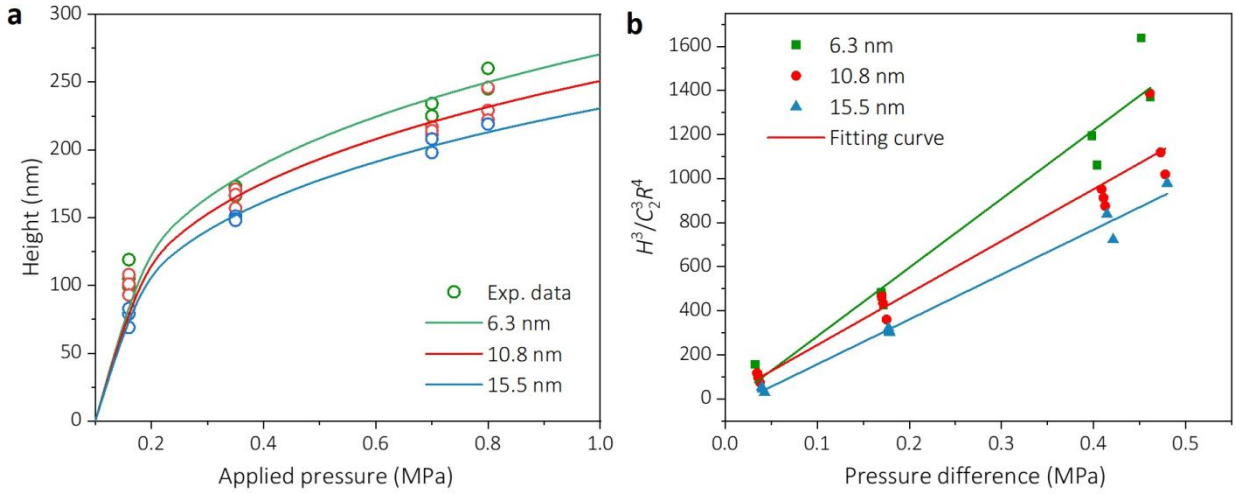

Figure S5. (a) VS_2 bubble height as a function of applied pressure at various thicknesses. (b) Normalized center deflection versus pressure difference for VS_2 bubbles with various thicknesses.

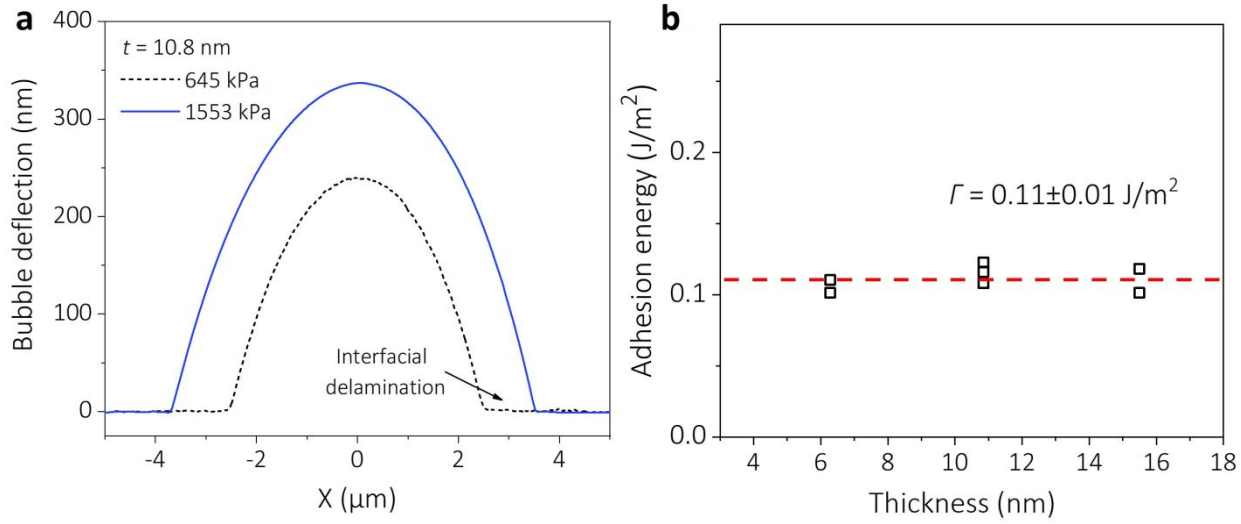

Figure S6. (a) AFM measurement of VS_2 bubble profile after the interfacial delamination. (b) Adhesion energy of VS_2 for different thicknesses.

During the bulging process, the bubble height can be expressed by[7]

$$H = C_2 \sqrt[3]{\frac{\Delta p R^4}{Et}} \tag{S1}$$

where C_2 is a constant as a function of the Poisson's ratio, which is 0.65 for VS_2. Such an H-Δp relationship is further evidenced by our AFM results for VS_2 bubbles with different thicknesses, suggesting the accuracy of measured Young's modulus. Once the delamination occurs, the adhesion energy is derived by seeking minima in the system free energy to achieve an equilibrium configuration:[8, 9]

$$\gamma = \frac{5}{4} C_1 \Delta p H = \frac{5}{4} C_1 \left(\frac{p_0 V_0}{V_0 + V_b} - p_e\right) H \tag{S2}$$

where $C_1 = 0.52$ is a constant depending on the Poisson's ratio, H is the bubble deflection at the center, p_0 is the applied pressure, V_0 is the volume of microcavity, V_b is the bubble volume and p_e is the atmosphere pressure. Based on the AFM measurement of bubble deflection and radius, the adhesion energy can be determined as ~0.11 J/m^2 as shown in Fig. S6b. This agrees well with the recent works reporting the adhesion energy between MoS_2 and Si/SiO_2 substrate (0.082-0.170 J/m^2).[10, 11]

At the critical pressure, the highest strain for a bubble can be obtained by combing Eq. (5), Eq. (S1) and Eq. (S2):

$$\varepsilon_{max} = A(\upsilon) \sqrt{\frac{4\gamma C_2^3}{5 C_1 E t}} \tag{S3}$$

S5. The function *f*(*N*) in two limiting cases

Two limiting cases are taken into account here to elucidate the interlayer shear effect on the bending rigidity. In the case of the perfect bonding between layers, the bending rigidity of multilayers is[12]

$$D_{\text{eff}} = ND_1 + \frac{Et_1{}^3}{12(1-\nu^2)}(N^3 - N) \tag{S4}$$

where D_1=4.87 eV is the calculated bending rigidity of monolayer VS_2. Based on Eq. (S2), we have

$$f(N) = \frac{12D_{eff}(1-\nu^2)}{Et_{total}^3} = 1 - \frac{1}{N^2} + \frac{12(1-\nu^2)D_1}{Et_1{}^3N^2} \tag{S5}$$

where $t_{\text{total}} = Nt_1$ and t_1 is the interlayer distance. For ultra-lubricated layers, the bending rigidity is simply expressed by

$$D_{eff} = ND_1 \tag{S6}$$

and thus

$$f(N) = \frac{12(1-\nu^2)D_1}{Et_1{}^3N^2} \tag{S7}$$

The theoretical limits predicted by Eqs. (S5) and (S7) are plotted as solid lines in Fig. 4g.

Reference

1. Li, J.; Medhekar, N. V.; Shenoy, V. B. Bonding Charge Density and Ultimate Strength of Monolayer Transition Metal Dichalcogenides. *J. Phys. Chem. C* **2013**, *117*, 15842-15848.
2. Kanoun, M. B.; Goumri-Said, S. Tailoring Optoelectronic Properties of Monolayer Transition Metal Dichalcogenide through Alloying. *Materialia* **2020**, *12*, 100708.
3. Wang, W.; Jiang, B.; Qian, C.; Lv, F.; Feng, J.; Zhou, J.; Wang, K.; Yang, C.; Yang, Y.; Guo, S. Pistachio-Shuck-Like MoSe2 /C Core/Shell Nanostructures for High-Performance Potassium-Ion Storage. *Adv. Mater.* **2018**, *30*, 1801812.
4. Bui, V. Q.; Pham, T. T.; Le, D. A.; Thi, C. M.; Le, H. M. A First-principles Investigation of Various Gas (CO, H2O, NO, and O2) Absorptions on a WS2 Monolayer: Stability and Electronic Properties. *J. Phys. Condens. Matter* **2015**, *27*, 305005.
5. Jing, Y.; Zhou, Z.; Cabrera, C. R.; Chen, Z. Metallic VS2 Monolayer: A Promising 2D Anode Material for Lithium Ion Batteries. *J. Phys. Chem. C* **2013**, *117*, 25409-25413.
6. Wang, W.; Sun, Z.; Zhang, W.; Fan, Q.; Sun, Q.; Cui, X.; Xiang, B. First-principles Investigations of Vanadium Disulfide for Lithium and Sodium Ion Battery Applications. *RSC Adv.* **2016**, *6*, 54874-54879.
7. Boddeti, N. G.; Koenig, S. P.; Long, R.; Xiao, J.; Bunch, J. S.; Dunn, M. L. Mechanics of Adhered, Pressurized Graphene Blisters. *J. Appl. Mech.* **2013**, *80*, 040909.
8. Koenig, S. P.; Boddeti, N. G.; Dunn, M. L.; Bunch, J. S. Ultrastrong Adhesion of Graphene Membranes. *Nat. Nanotechnol.* **2011**, *6*, 543-546.
9. Wang, G., Interfacial Friction and Adhesion Between Graphene and Silicon. In *Characterization and Modification of Graphene-Based Interfacial Mechanical Behavior*, Springer: Singapore, 2020; pp 67-96.
10. Sanchez, D. A.; Dai, Z.; Wang, P.; Cantu-Chavez, A.; Brennan, C. J.; Huang, R.; Lu, N. Mechanics of Spontaneously Formed Nanoblisters Trapped by Transferred 2D Crystals. *Proc. Natl. Acad. Sci. USA* **2018**, *115*, 7884-7889.
11. Deng, S.; Gao, E.; Xu, Z.; Berry, V. Adhesion Energy of MoS2 Thin Films on Silicon-Based Substrates Determined via the Attributes of a Single MoS2 Wrinkle. *ACS Appl. Mater. Interfaces* **2017**, *9*, 7812-7818.
12. Gao, W.; Huang, R. Effect of Surface Roughness on Adhesion of Graphene Membranes. *J. Phys. D Appl. Phys.* **2011**, *44*, 452001.